Original Article

The value of ^{123}I-MIBG xSPECT/CT quantitative parameters in the diagnosis of bone metastasis in pediatric neuroblastoma patients

Xiaoya Wang, Guanyun Wang, Ziang Zhou, Ying Kan, Jigang Yang

Nuclear Medicine Department, Beijing Friendship Hospital, Affiliated to Capital Medical University, Beijing, China

Contributions: (I) Conception and design: X Wang, G Wang, J Yang; (II) Administrative support: Y Kan, J Yang; (III) Provision of study materials or patients: X Wang, G Wang, Y Kan; (IV) Collection and assembly of data: X Wang, G Wang, Z Zhou; (V) Data analysis and interpretation: X Wang, G Wang; (VI) Manuscript writing: All authors; (VII) Final approval of manuscript: All authors.

Correspondence to: Jigang Yang, MD. Nuclear Medicine Department, Beijing Friendship Hospital, Affiliated to Capital Medical University, 95 Yong'an Road, Xicheng District, Beijing 100032, China. Email: yangjigang@ccmu.edu.cn.

Background: The diagnostic value of quantitative single-photon emission computed tomography/computed tomography (xSPECT/CT) in the screening of bone metastases of various malignant tumors varies. This study investigated the differential diagnostic value of quantitative parameters of ^{123}I-metaiodobenzylguanidine (^{123}MIBG) xSPECT/CT imaging in the diagnosis of bone metastasis in pediatric neuroblastoma (NB) patients.

Methods: In this retrospective cohort study, the ^{123}I-MIBG xSPECT/CT images of 125 children with NB confirmed by pathology at Beijing Friendship Hospital from March 2022 to December 2023 were assessed. A Spearman correlation analysis was conducted to assess the factors influencing normal bone quantitative parameters, and differences in the standardized uptake values (SUVs), including the maximum standardized uptake value (SUVmax), average standardized uptake value (SUVavg), minimum standardized uptake value (SUVmin), and peak standardized uptake value (SUVpeak), between metastatic bone lesions and normal bone were compared using the Mann-Whitney *U* test. Receiver operating characteristic (ROC) curves were used to determine the optimal cut-off values of the SUVs in the diagnosis of metastatic bone lesions. The above indexes were compared via a visual analysis, and using the chi-square test. The clinical parameters and semi-quantitative indexes of xSPECT/CT were also analyzed using univariate and multivariate methods.

Results: The study cohort comprised 75 girls and 50 boys with an average age of 5.94 years (0.6–9 years). The SUVs of metastatic bone lesions were significantly higher than those of normal bone (P<0.0001), but there was no statistically significant difference in the SUV values of metastatic bone lesions among the different Curie score subzones (P>0.05). The area under the curve (AUC) values for the SUVmax, SUVavg, SUVmin, and SUVpeak were 0.946 [95% confidence interval (CI): 0.921–0.971], 0.962 (95% CI: 0.939–0.984), 0.953 (95% CI: 0.928–0.978), and 0.959 (95% CI: 0.936–0.982), respectively (P<0.0001). The optimal diagnostic thresholds identified for the SUVmax, SUVavg, SUVmin, and SUVpeak were 0.39, 0.36, 0.19 and 0.35, respectively. The SUVavg was the best index among the different Curie score subzones, and the specificity of the quantitative analysis in diagnosing bone metastasis in NB patients was better than that of the visual analysis. We also showed that tumor stage and neuron specific enolase (NSE) levels are important factors influencing the diagnosis of bone metastasis. There was no statistically significant difference in the SUV values for normal bone among different physical parameters (P>0.05).

Conclusions: A SUVavg above 0.36 g/mL in NB patients had the best efficacy in the diagnosis of bone metastasis in NB patients. Quantitative indexes of xSPECT/CT had better specificity in the diagnosis of bone metastasis in NB patients than the visual analysis. ^{123}I-MIBG xSPECT/CT imaging can increase the diagnostic confidence of bone metastasis in NB.

Keywords: Neuroblastoma (NB); bone metastasis; single-photon tomography; X-ray computer

Submitted Jun 20, 2024. Accepted for publication Oct 12, 2024. Published online Nov 27, 2024.
doi: 10.21037/qims-24-1251
View this article at: https://dx.doi.org/10.21037/qims-24-1251

Introduction

Neuroblastoma (NB) is the malignant tumor with the highest mortality rate in children, and accounts for approximately 15% of all pediatric malignancy-related deaths (1). It can occur in any part of the sympathetic nervous system; however, the majority of primary tumors (65–70%) occur in the abdomen, most commonly in the adrenal glands (2). Studies have shown that patients with primary sites in the adrenal glands have a higher risk of recurrence and metastasis than those with primary sites in other locations (3). NB is highly susceptible to distant metastasis, most commonly in the bone, distant lymph nodes, and liver (4). Under the International Neuroblastoma Staging System (INSS) (5), NB with bone metastasis is classified as stage IV, which necessitates adjustments in the treatment plan, and indicates a potential unfavorable prognosis for patients. Therefore, the early detection of bone metastasis is crucial for the subsequent treatment and prognosis of children with NB.

The routine evaluation of bone metastasis in NB primarily includes X-ray, computed tomography (CT), and magnetic resonance imaging (MRI), all of which are non-specific examinations. These methods can assess the location of metastatic lesions, and the relationship between lesions and surrounding tissues, but usually cannot accurately determine the nature of the lesions. Functional imaging modalities of nuclear medicine, such as ^{99m}Tc-methylene diphosphonate (^{99m}Tc-MDP) bone scintigraphy and ^{18}F-fluorodeoxyglucose (^{18}F-FDG) positron emission tomography-computed tomography (PET/CT) scans, can be used to evaluate the location, extent, and activity of residual lesions with respect to the metastatic characteristics of NB, but these modalities have low accuracy, and are prone to false positives or false negatives.

^{123}I-metaiodobenzylguanidine (MIBG) is currently the preferred radiopharmaceutical method for imaging pediatric NB due to its high sensitivity and specificity (6,7). A variety of semi-quantitative scoring systems have been developed to assess tumor load and to quantify response to therapy, of which the Curie score, which can be used to determine patient prognosis and the efficacy of NB treatment, is the most widely used (8). However, it is based on ^{123}I-MIBG planar imaging, which may yield false-negative results due to its limited spatial resolution, and physiological or non-neoplastic MIBG uptake is not always easy to distinguish from pathological uptake, which could potentially lead to false-positive results (9). ^{123}I-MIBG single-photon emission computed tomography/computed tomography (xSPECT/CT) can significantly improve the accuracy of NB diagnosis; however, due to background noise, it is also relatively difficult to identify NB metastatic lesions and monitor prognosis based only on a visual analysis of MIBG planar or tomographic imaging (10). Thus, further research needs to be conducted to determine how to identify bone metastatic lesions using relatively objective indexes, and thus improve the specificity and accuracy of diagnosis.

Siemens xSPECT/CT technology is based on the Symbia Intevo system. This new high-definition bone imaging technique uses segmented CT information to reconstruct reference frames and integrate data from large matrix SPECT acquisitions. This technology enhances the resolution of SPECT/CT, and allows for the quantification of MIBG uptake to obtain standardized uptake values (SUVs) and other parameters (11). Due to the continuous improvement of image reconstruction algorithms and the application of complex compensation techniques in the correction of photon attenuation and scattering, quantitative xSPECT/CT can now accurately restore the display of internal radiation distribution of the lesion and improve the detection of small lesions, which has led to significant progress in its clinical applications (12). Quantitative xSPECT/CT has demonstrated varying degrees of diagnostic value of ^{99m}Tc-MDP in screening for bone metastases from various malignant tumors, such as prostate cancer (13), lung cancer (14), and breast cancer (15). However, there is still a lack of research on the use of ^{123}I-MIBG xSPECT/CT imaging in the diagnosis of NB metastasis.

Therefore, this study analyzed the quantitative parameters of bone metastasis of NB and further investigated the value of quantitative ^{123}I-MIBG xSPECT/CT imaging in diagnosing bone metastasis in pediatric NB patients. We present this article in accordance with the STROBE reporting checklist (available at https://qims.amegroups.com/article/view/10.21037/qims-24-1251/rc).

Methods

Patients

A retrospective cohort study was conducted on 414 pediatric patients with NB and clinical suspicion of bone metastasis who underwent quantitative ^{123}I-MIBG xSPECT/CT imaging at Beijing Friendship Hospital from March 2022 to December 2023. To be eligible for inclusion in this study, the patients had to meet the following inclusion criteria: (I) have a diagnosis of NB based on pathological or clinical criteria; (II) be aged <18 years; and (III) have undergone treatment according to the Multidisciplinary Treatment Guidelines for NB developed by the Chinese Children's Cancer Group of the China Anti-Cancer Association (16). Patients were excluded from the study if they met any of the following exclusion criteria: (I) had an unclear diagnosis of NB or had other tumors; (II) had incomplete medical records; and/or (III) were unable to cooperate with the follow-up.

A total of 125 patients were enrolled in the study. The following clinical data were recorded: age, sex, weight, height, primary tumor site, histologic type and stage, MYCN amplification, 11q aberration, neuron specific enolase (NSE) level one week before xSPECT/CT imaging, and current treatment status. The INSS (17) and the Children's Oncology Group Classification were used to determine stage and histologic type respectively. All patients were followed-up for a minimum period of six months.

The study was conducted in accordance with the Declaration of Helsinki (as revised in 2013). The study was approved by the local ethical review board of Beijing Friendship Hospital of Capital Medical University (No. 2022-P2-314-01). Informed consent was obtained from all the patients' parents or legal guardians.

xSPECT/CT acquisition

The ^{123}I-MIBG xSPECT/CT imaging was performed using the xSPECT/CT system (Siemens Symbia Intevo T16). To close the thyroid gland, Lugol's iodine solution was administered from 3 days before to 2 days after the imaging procedure. Patients received an intravenous injection of ^{123}I-MIBG at a dose of 5.2 MBq/kg (37–370 MBq), adjusted based on their age, height, and weight. Details of the full syringe, empty syringe, and injection time were simultaneously recorded. Anteroposterior whole-body planar imaging with ^{123}I-MIBG and local xSPECT/CT were performed 24 hours post-injection.

xSPECT/CT was primarily used to characterize suspicious lesions or lesions that could not be identified by planar imaging. In instances in which planar imaging yielded negative results, local xSPECT/CT imaging of the surgical area was conducted. SPECT data acquisition involved acquiring images with 60 steps of 10 s/step, 360°, and a 256×256 matrix. The CT scanning parameters were as follows: tube voltage: 110 keV; tube current: 90 mA; slice thickness: 3 mm; and pitch value: 0.8 mm. The acquired xSPECT images underwent post-processing using SyngoMIVB21A software; iterative reconstruction following CT attenuation correction was applied before fusion with the CT images to generate the final xSPECT/CT images.

Image analysis

The images were assessed by two experienced nuclear medicine physicians (with more than 5 years of experience each) using the workstation (Syngo Multimodality Workplace, Siemens) without access to original scan reports or other clinical information, and any discrepancies were resolved through mutual discussion until consensus was reached. For the analysis, cubic volumes of interest >10 mm were placed on the cross-sectional, sagittal, and coronal planes of the regions with bone abnormalities, and abnormal radiotracer accumulation was identified on the CT images (*Figure 1*). The software automatically calculated the maximum standardized uptake value (SUVmax), average standardized uptake value (SUVavg), minimum standardized uptake value (SUVmin), and peak standardized uptake value (SUVpeak) of the lesions. The SUV formula is expressed as follows:

SUV = specific activity of the region of interest (kBq/mL) × weight (kg)/injection dose (MBq).

A diagnosis of bone metastasis was established based on the following: (I) a pathological diagnosis (based on local bone biopsy); (II) imaging examination results, including ^{123}I-MIBG imaging, ^{18}F-FDG PET/CT, ultrasound, enhanced CT and MRI; and (III) the patient's medical history and long-term follow-up results. The selection criteria for normal bone relied on lumbar vertebrae 3 as the reference standard, characterized by the uniform distribution of radioactivity, and the absence of abnormal changes in CT scans. In cases where L3 was affected, adjacent lumbar vertebrae L1–2 were used as the reference standard (18).

Statistical analysis

The continuous variables are reported as the mean ± standard deviation, or the median and interquartile range.

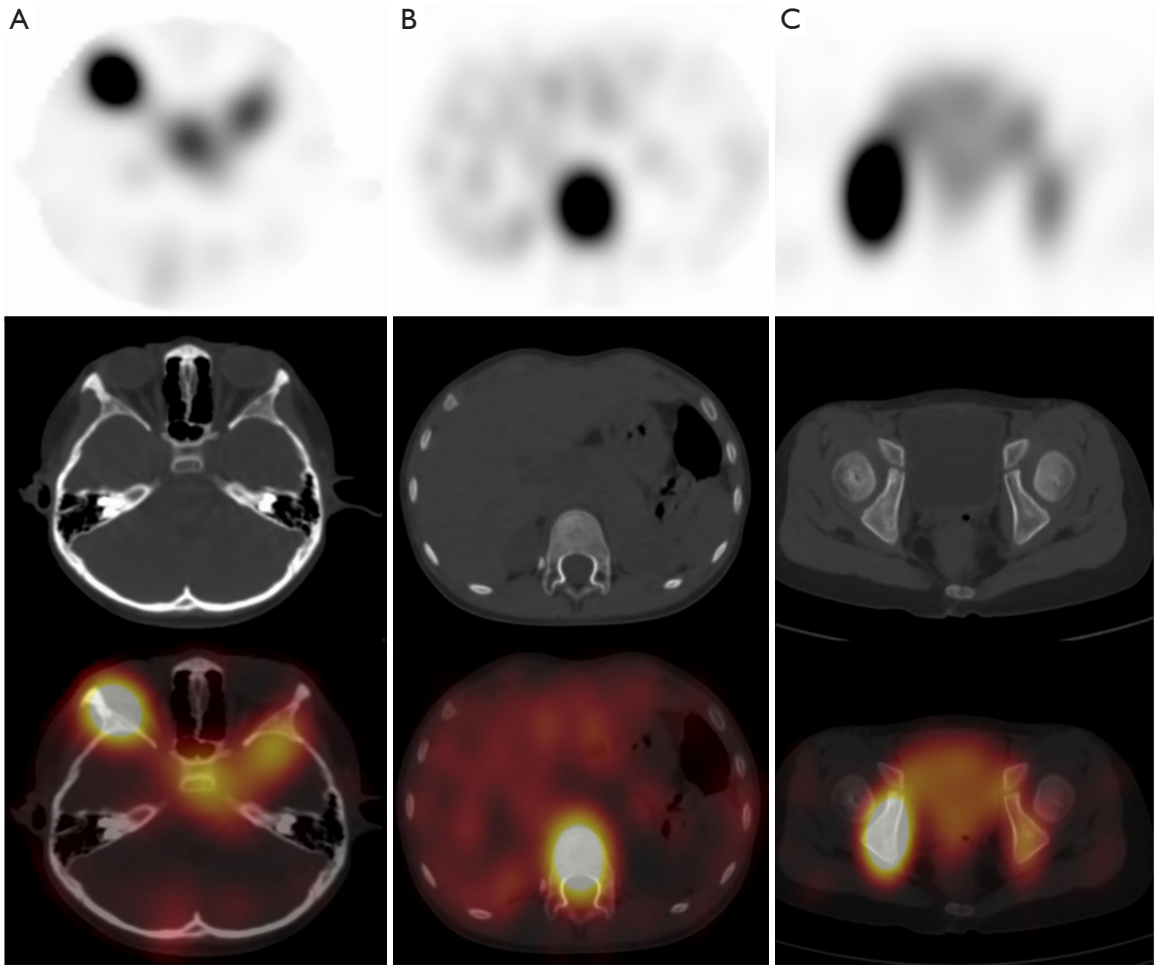

Figure 1 Representative ^{123}I-MIBG xSPECT/CT images of a patient with positive bone metastasis results. In a 7-year-old girl diagnosed with NB in the left adrenal gland, xSPECT/CT revealed enhanced contrast uptake in the lateral wall of the orbit (A), spine (B) and pelvis (C). The larger one in the right iliac bone corresponded to the SUVmax, SUVavg, SUVmin, and SUVpeak values of 9.34, 7.48, 4.99, and 8.98 respectively; subsequently confirming the presence of bone metastasis. ^{123}I-MIBG, ^{123}I-metaiodobenzylguanidine; xSPECT/CT, single-photon emission computed tomography/computed tomography; NB, neuroblastoma; SUVmax, maximum standardized uptake value; SUVavg, average standardized uptake value; SUVmin, minimum standardized uptake value; SUVpeak, peak standardized uptake value.

The categorical variables are reported as the count and percentage. A Spearman correlation analysis was conducted to assess the association between the normal SUV and physical variables. Intergroup comparisons were conducted using the Mann-Whitney *U* test, while multi-group comparisons were conducted using the Kruskal-Wallis *H* test. Receiver operating characteristic (ROC) curves were constructed to determine the optimal cut-off values of the SUVs for distinguishing between metastatic and normal lesions, with corresponding area under the curve (AUC) values, sensitivity, and specificity derived. A univariate analysis was performed of the clinical information and imaging characteristics of the patients, after which, any statistically significant variables were included in the multivariate logistic regression analysis. The statistical analyses were carried out using SPSS 26.0 software. All the statistical tests were two-sided, and a significance level of $P<0.05$ was considered statistically significant.

Results

Clinical parameters

Based on the inclusion and exclusion criteria, 125 pediatric

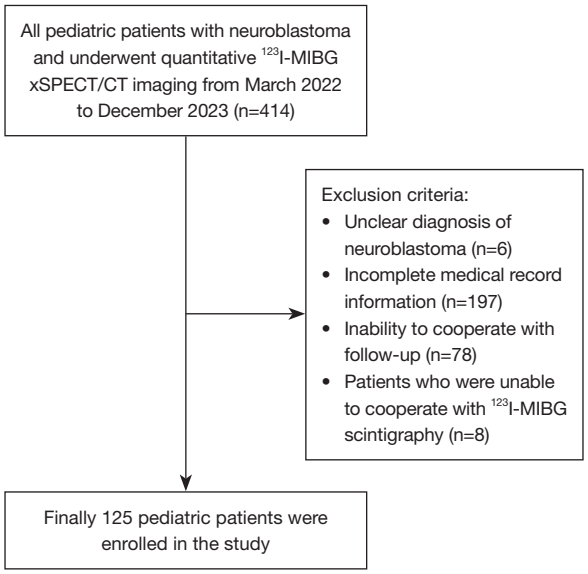

Figure 2 Flow diagram of patient inclusion, with reasons for exclusion, and the total study population. ^{123}I-MIBG, ^{123}I-metaiodobenzylguanidine; xSPECT/CT, single-photon emission computed tomography/computed tomography.

patients with NB who underwent ^{123}I-MIBG xSPECT/CT imaging were included in the study. The study cohort comprised 75 girls and 50 boys. The patients had an average age of 5.94 years (0.6–9 years) (*Figure 2*). All the patients received standardized treatment based on their risk group classification. The primary tumor sites included retroperitoneum (61 cases in the adrenal region, and 25 cases outside the adrenal region), as well as other regions (39 cases). Among the NB patients, 65 were diagnosed with NB and 60 were diagnosed with ganglioneuroblastoma. Pathological grading revealed that the majority of tumors were classified as high risk (n=98), while a smaller proportion fell into other grades, with 22 classified as median risk, and five classified as low risk (*Table 1*). Ultimately, a total of 329 metastatic lesions were confirmed to be bone metastases at final diagnosis.

Differences among the SUV measurements of metastatic subzones

The SUVmax, SUVavg, SUVmin, and SUVpeak of all bone metastatic lesions were significantly higher than those of normal bone lesions (P<0.0001). The children's metastatic sites were categorized based on the Curie score, with 69 bone metastatic lesions in the head (zone 1), 175 in the

Table 1 Characteristics of the NB patients

Characteristics	Values
Sex	
Female	75 (60.0)
Male	50 (40.0)
Age (years)	
Mean ± SD	5.94±3.54
Range	0.6–9
Treatment status	
Induction therapy	31 (24.8)
Maintenance therapy	77 (61.6)
Consolidation therapy	17 (13.6)
Primary tumor location	
Adrenal gland	61 (48.8)
Retroperitoneum	25 (20.0)
Mediastinum	27 (21.6)
Pelvis	3 (2.4)
Others	9 (7.2)
Histologic type	
Neuroblastoma	65 (52.0)
Ganglioneuroblastoma	60 (48.0)
Risk stratification	
High risk	98 (78.4)
Median risk	22 (17.6)
Low risk	5 (4.0)
INSS stage	
IV	99 (79.2)
III	14 (11.2)
II	11 (8.8)
I	1 (0.8)
MYCN amplification	
Yes	38 (30.4)
No	87 (69.6)
11q aberration	
Yes	71 (56.8)
No	54 (43.2)
NSE	
Normal	60 (48.0)
Abnormal	65 (52.0)

Data are presented as n (%) unless otherwise specified. NB, neuroblastoma; SD, standard deviation; INSS, International Neuroblastoma Staging System; NSE, neuron specific enolase.

Table 2 SUV measurements for normal bone and different metastatic subzones

SUV	Normal bone (n=123)	Head metastasis (n=69)	Trunk metastasis (n=175)	Limbs metastasis (n=85)	P
SUVmax	0.22 (0.13, 0.30)	0.86 (0.52, 1.85)	0.99 (0.63, 1.60)	0.83 (0.54, 1.70)	<0.0001
SUVavg	0.12 (0.07, 0.20)	0.71 (0.46, 1.48)	0.79 (0.51, 1.25)	0.66 (0.46, 1.27)	<0.0001
SUVmin	0.08 (0.05, 0.13)	0.53 (0.31, 1.00)	0.58 (0.34, 0.91)	0.46 (0.31, 0.81)	<0.0001
SUVpeak	0.16 (0.09, 0.23)	0.78 (0.47, 1.70)	0.92 (0.59, 1.51)	0.78 (0.49, 1.57)	<0.0001

Data are presented as the median (interquartile range). SUV, standardized uptake value; SUVmax, maximum standardized uptake value; SUVavg, average standardized uptake value; SUVmin, minimum standardized uptake value; SUVpeak, peak standardized uptake value.

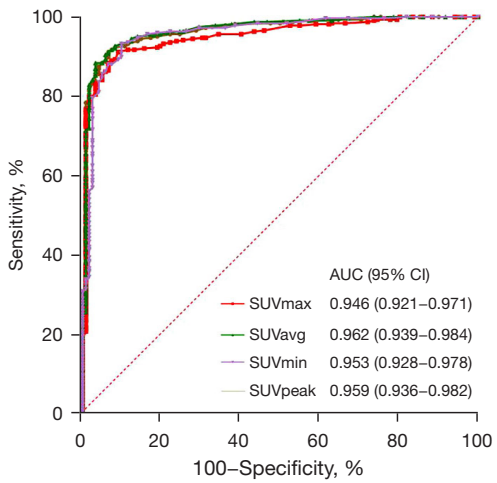

Figure 3 ROC curves depicting SUV measurements for the detection of bone metastasis in NB. SUVmax, maximum standardized uptake value; SUVavg, average standardized uptake value; SUVmin, minimum standardized uptake value; SUVpeak, peak standardized uptake value; AUC, area under the curve; CI, confidence interval; ROC, receiver operating characteristic; SUV, standardized uptake value; NB, neuroblastoma.

trunk (zones 2–5), and 85 in the limbs (zones 6–9) (*Table 2*). Nevertheless, no statistically significant difference was observed in the SUV measurements of bone metastatic foci among the different subzones (P>0.05).

Value of 123I-MIBG xSPECT/CT in the evaluation of NB bone metastasis

The ROC curves of the SUVmax, SUVavg, SUVmin, and SUVpeak were generated based on measurements of normal bone and bone metastasis (*Figure 3*). The diagnostic utility of the SUV in discriminating between normal bone and lesions was assessed, and the AUC values of the SUVmax, SUVavg, SUVmin, and SUVpeak, were 0.946 [95% confidence interval (CI): 0.921–0.971], 0.962 (95% CI: 0.939–0.984), 0.953 (95% CI: 0.928–0.978), and 0.959 (95% CI: 0.936–0.982), respectively. The sensitivity was 91.2%, 88.4%, 93.3% and 91.2%, and the specificity was 90.2%, 95.9%, 89.4% and 92.7% for the SUVmax, SUVavg, SUVmin, and SUVpeak, respectively. All these differences reached statistical significance with P values <0.0001. The optimal diagnostic thresholds identified for the SUVmax, SUVavg, SUVmin, and SUVpeak were 0.39, 0.36, 0.19 and 0.35, respectively. The ROC curves comparing different metastatic sites in children according to Curie score partitioning were also analyzed. Ultimately, among all the partitions examined, the SUVavg had the highest diagnostic efficacy (*Table 3*). Additionally, we observed a total of 332 sites of radiotracer distribution on ^{123}I-MIBG xSPECT/CT imaging, of which 325 cases were consistent with the final diagnosis. The visual analysis demonstrated a specificity of 94.6% for diagnosing bone metastasis of NB, while the SUVavg parameter exhibited a specificity of 95.9%.

Diagnostic factors for NB bone metastasis

In the univariate analysis, tumor location, risk stratification, INSS stage, 11q aberration, NSE level, and SUV measurements were identified as statistically significant factors for diagnosing bone metastatic lesions. However, it should be noted that the effect estimates for some of these clinical factors were relatively small. In the multifactorial analysis, INSS stage, NSE level, and SUV quantitative measurements were significant risk factors in diagnosing bone metastatic lesions (*Table 4*).

Relationship between normal bone SUV and physical parameters

The normal bone SUV values did not show statistically significant differences across different physical parameters

Table 3 AUC values for the SUV measurements across distinct metastatic subzones

Subzones	SUVmax	SUVavg	SUVmin	SUVpeak
Head	0.927 (0.884–0.970)	0.947 (0.911–0.983)	0.942 (0.904–0.980)	0.944 (0.907–0.980)
Trunk	0.956 (0.930–0.982)	0.968 (0.946–0.991)	0.960 (0.935–0.985)	0.966 (0.943–0.990)
Limbs	0.940 (0.905–0.975)	0.960 (0.933–0.986)	0.947 (0.917–0.978)	0.957 (0.929–0.985)

Data are presented as AUC (95% CI). AUC, area under the curve; SUV, standardized uptake value; SUVmax, maximum standardized uptake value; SUVavg, average standardized uptake value; SUVmin, minimum standardized uptake value; SUVpeak, peak standardized uptake value; CI, confidence interval.

Table 4 Univariate and multivariate analysis of the diagnostic factors associated with bone metastasis

Characteristics	Univariate analysis			Multivariate analysis		
	OR	95% CI	P	OR	95% CI	P
Inductive treatment	0.950	0.521–1.732	0.867	1.944	0.763–4.954	0.164
Adrenal gland	0.630	0.416–0.956	0.030	1.565	0.793–3.090	0.196
Neuroblastoma	1.431	0.128–16.042	0.771	1.025	0.520–2.023	0.942
High risk	0.338	0.190–0.600	0.0001	0.225	0.043–1.179	0.078
IV stage	0.191	0.097–0.377	0.0001	13.970	1.885–103.543	0.010
MYCN amplification	1.084	0.692–1.699	0.725	0.956	0.465–1.968	0.904
11q aberration	1.534	1.001–2.349	0.049	1.195	0.588–2.430	0.622
NSE abnormal	2.084	1.367–3.177	0.0001	2.014	1.014–4.002	0.046
SUVmax	10.864	5.603–21.063	0.0001	–	–	0.0001
SUVavg	40.471	16.202–101.093	0.0001	–	–	0.0001
SUVmin	71.057	23.156–218.051	0.0001	–	–	0.0001
SUVpeak	18.436	8.628–39.394	0.0001	–	–	0.0001

NSE, neuron specific enolase; SUVmax, maximum standardized uptake value; SUVavg, average standardized uptake value; SUVmin, minimum standardized uptake value; SUVpeak, peak standardized uptake value; OR, odds ratio; CI, confidence interval.

[i.e., gender, age, height, weight, and body mass index (BMI)] (P>0.05, *Table 5*).

Discussion

Our study investigated the potential use of ^{123}I-MIBG xSPECT/CT in the diagnosis of 329 bone metastatic lesions in 125 pediatric patients with NB. We observed that a focal MIBG uptake SUVavg >0.36 g/mL was highly indicative of metastasis in NB patients, and the quantitative analysis significantly enhanced the specificity of diagnosing bone metastasis in NB patients compared to the visual analysis. To our knowledge, this is the first study to show that quantitative parameters obtained from ^{123}I-MIBG xSPECT/CT can assist in the diagnosis of bone metastatic lesions of NB.

NB originates in the sympathetic nervous system and involves a wide range of sites, most often the adrenal gland (19). Studies have shown that patients with the primary site in the adrenal gland have a higher risk of recurrence and metastasis than patients with other primary sites (20,21). In this study, of the 125 children with bone metastasis, the primary site was the adrenal gland in 61 (48.8%) patients, which is consistent with figures from previous reports. NB exhibits a high susceptibility to recurrence and metastasis (21). The 5-year survival rate of NB patients with bone metastasis is approximately 41.3% (22). The detection of bone metastasis at any location leads to its classification as stage IV according to INSS, necessitating a modification in treatment approach. Some low-risk children experience spontaneous resolution;

Table 5 Correlation analysis between normal bone SUV and physical parameters

SUV	Gender		Age		Height		Weight		BMI	
	r	P	r	P	r	P	r	P	r	P
SUVmax	0.110	0.228	0.010	0.911	–0.016	0.860	0.001	0.991	0.019	0.834
SUVavg	0.103	0.255	–0.071	0.436	–0.104	0.253	–0.102	0.261	–0.060	0.508
SUVmin	0.139	0.124	–0.113	0.213	–0.153	0.092	–0.162	0.073	–0.123	0.176
SUVpeak	0.044	0.629	0.007	0.936	–0.016	0.857	–0.015	0.867	–0.011	0.900

SUV, standardized uptake value; SUVmax, maximum standardized uptake value; SUVavg, average standardized uptake value; SUVmin, minimum standardized uptake value; SUVpeak, peak standardized uptake value; BMI, body mass index.

however, those classified as high risk face an unfavorable prognosis even after undergoing induction, consolidation, and maintenance therapy (23). Thus, the assessment of the occurrence of bone metastasis is of great importance in determining treatment strategies and prognostic outcomes.

The clinical diagnosis of bone metastasis typically involves a comprehensive analysis of CT, MRI, bone scintigraphy, and clinical symptoms during follow-up. However, the limited sensitivity of conventional imaging techniques poses challenges in the early detection of bone metastatic lesions and prolongs the diagnostic process. Consequently, there is an urgent need for a non-invasive and efficient method to enable the early diagnosis of bone metastatic lesions and the accurate evaluation of treatment efficacy.^{123}I-MIBG imaging, serving as a primary functional modality for assessing NB, exhibits superior sensitivity and specificity in detecting bone metastasis than ^{99m}Tc-MDP bone scintigraphy (24), enhancing the characterization of the disease extent and distribution. Various semi-quantitative scoring systems, such as the Curie score, have been employed to systematically evaluate the severity and distribution of bone metastasis in NB (25). Planar imaging forms the basis of ^{123}I-MIBG assessment, where any uptake beyond the normal radiotracer distribution (particularly focal uptake) is indicative of disease infiltration. Recent studies have shown that ^{123}I-MIBG SPECT/CT can significantly enhance diagnostic sensitivity, specificity, and accuracy in NB diagnosis (10,26). However, conventional SPECT/CT lacks objective quantitative metrics and can only be analyzed qualitatively (27).

xSPECT/CT is an innovative iterative reconstruction algorithm developed on the basis of fusion SPECT/CT, which generates laminar images with voxel values representing activity. The voxel values can be converted to parameters by extracting the delineated volume from the image (28). It has shown varying degrees of diagnostic value in the screening of complex and small anatomical lesions (29), joint lesions (12), and bone metastases (13,30), and in the monitoring of compression fractures. Studies have confirmed that ^{99m}Tc-MDP xSPECT/CT improves the diagnostic accuracy and consistency of diagnosing NB bone metastasis while enhancing clinical effectiveness. However, there is currently a lack of research on the use of ^{123}I-MIBG xSPECT/CT imaging for the diagnosis of NB metastasis.

Our study validated the use of a novel algorithm in xSPECT/CT reconstruction, which effectively enhanced the specificity of bone metastasis diagnosis in NB patients. This advancement facilitates disease monitoring and prognosis evaluation in pediatric patients. Quantitative xSPECT/CT enables the accurate differentiation of the physiological uptake of surrounding lesions (e.g., orbit, ribs, and sacrum) by reducing image background noise. Consequently, it improves the precise diagnosis of bone metastatic lesions to some extent. This cut-off value offers additional diagnostic value, as a focal MIBG SUVavg uptake >0.36 g/mL is highly indicative of metastasis in NB patients, and thus could help clinicians to accurately identify bone metastasis in NB. This finding further strengthens the clinical significance of MIBG imaging in the diagnosis of bone metastatic lesions in NB patients. In this study, we employed the Curie score for the semi-quantitative assessment of MIBG uptake in systemic bone metastatic lesions. However, it should be noted that due to varying lesion sizes, potential partial volume effects between different subdivisions might influence visualizer uptake measurements. Nevertheless, we found no statistically significant differences in the SUV values among these regions.

We also found that tumor stage, NSE level, and the SUV measurement parameters of ^{123}I-MIBG xSPECT/CT were significant factors influencing the diagnosis of

bone metastasis. Our study included pediatric NB patients who were at different treatment stages according to the consensus protocol for NB diagnosis. This variability might have affected the uptake of MIBG in bone metastatic lesions. Previous treatments could potentially induce sclerosis, reduce vascularity, or cause other alterations in the tumor microenvironment, all of which can influence the uptake of imaging agents (14). However, the treatment status of the children was not identified as a significant influencing factor in the diagnosis of bone metastatic lesions in our study. The changes in the SUVs observed for bone metastatic lesions may provide more valuable guidance for NB patients in clinical practice; this aspect will be explored in future investigations. Additionally, Rogasch *et al.* were the first to undertake a stratified study of pediatric NB patients based on quantitative parameters obtained from the primary tumor site using ^{123}I-MIBG xSPECT/CT. This approach is closely associated with the selection of subsequent treatment regimens and prognosis evaluation in children (31). Therefore, investigating whether the metabolic parameters of bone metastasis have additional prognostic value for NB is crucial and will be further investigated in our follow-up study.

This study provided the first validation of the diagnostic value of quantitative ^{123}I-MIBG xSPECT/CT imaging for bone metastatic lesions in pediatric NB patients. However, it is important to acknowledge certain limitations associated with this study. First, its retrospective design and small sample size restrict the generalizability of the findings. Second, only body sites in the field of view of ^{123}I-MIBG xSPECT/CT were compared, and lesions without corresponding tomographic images were excluded from the final analysis. The study highlights the reliance of nuclear medicine physicians on subjective judgments, which could introduce variability and potential bias in the diagnostic outcomes. Third, most of the bone metastatic lesions were not pathologically confirmed; thus, continued follow-up is required to further support and validate these findings. Fourth, it should be noted that there was no significant correlation between the quantitative parameters of normal bone in ^{123}I-MIBG xSPECT/CT imaging and the overall condition of pediatric patients; this discrepancy may be attributed to factors such as patient characteristics and the contrast agent used. Finally, 10% of NB are MIBG non-avid, and ^{123}I-MIBG imaging has relatively low spatial resolution. We primarily focused on MIBG-avid lesions, and did not consider MIBG non-avid lesions. In the future, we intend to conduct a larger scale prospective study and incorporate other imaging examinations to make the conclusions of the study more comprehensive.

Conclusions

The use of ^{123}I-MIBG xSPECT/CT scintigraphy has incremental value in the diagnosis of NB metastasis, and can serve as a diagnostic aid for visual assessments. An SUVavg >0.36 g/mL in suspicious bone regions of NB patients is highly indicative of metastasis. Moreover, the specificity of the quantitative analysis in diagnosing NB bone metastasis was better than that of the visual analysis; thus, it can be used to improve the accuracy of diagnosing metastatic bone lesions.

Acknowledgments

The authors would like to thank the staff at the Nuclear Medicine Department, Beijing Friendship Hospital, Affiliated to Capital Medical University for their assistance in this study.

Footnote

Reporting Checklist: The authors have completed the STROBE reporting checklist. Available at https://qims.amegroups.com/article/view/10.21037/qims-24-1251/rc

Funding: This study was supported by grants from the Natural Science Foundation of Beijing (No. 7232031), and the National Natural Science Foundation of China (No. 82272034).

Conflicts of Interest: All authors have completed the ICMJE uniform disclosure form (available at https://qims.amegroups.com/article/view/10.21037/qims-24-1251/coif). The authors have no conflicts of interest to declare.

Ethical Statement: The authors are accountable for all aspects of the work in ensuring that questions related to the accuracy or integrity of any part of the work are appropriately investigated and resolved. The study was conducted in accordance with the Declaration of Helsinki (as revised in 2013). This retrospective cohort study was approved by the local ethical review board of Beijing Friendship Hospital of Capital Medical University (No. 2022-P2-314-01). Informed consent forms were signed by all participating patients' parents or legal guardians.

References

1. Chung C, Boterberg T, Lucas J, Panoff J, Valteau-Couanet D, Hero B, Bagatell R, Hill-Kayser CE. Neuroblastoma. Pediatr Blood Cancer 2021;68 Suppl 2:e28473.
2. Park JR, Eggert A, Caron H. Neuroblastoma: biology, prognosis, and treatment. Hematol Oncol Clin North Am 2010;24:65-86.
3. Vo KT, Matthay KK, Neuhaus J, London WB, Hero B, Ambros PF, Nakagawara A, Miniati D, Wheeler K, Pearson AD, Cohn SL, DuBois SG. Clinical, biologic, and prognostic differences on the basis of primary tumor site in neuroblastoma: a report from the international neuroblastoma risk group project. J Clin Oncol 2014;32:3169-76.
4. DuBois SG, Kalika Y, Lukens JN, Brodeur GM, Seeger RC, Atkinson JB, Haase GM, Black CT, Perez C, Shimada H, Gerbing R, Stram DO, Matthay KK. Metastatic sites in stage IV and IVS neuroblastoma correlate with age, tumor biology, and survival. J Pediatr Hematol Oncol 1999;21:181-9.
5. Brodeur GM, Seeger RC, Barrett A, Berthold F, Castleberry RP, D'Angio G, De Bernardi B, Evans AE, Favrot M, Freeman AI. International criteria for diagnosis, staging, and response to treatment in patients with neuroblastoma. J Clin Oncol 1988;6:1874-81.
6. Matthay KK, Shulkin B, Ladenstein R, Michon J, Giammarile F, Lewington V, Pearson AD, Cohn SL. Criteria for evaluation of disease extent by (123) I-metaiodobenzylguanidine scans in neuroblastoma: a report for the International Neuroblastoma Risk Group (INRG) Task Force. Br J Cancer 2010;102:1319-26.
7. Samim A, Tytgat GAM, Bleeker G, Wenker STM, Chatalic KLS, Poot AJ, Tolboom N, van Noesel MM, Lam MGEH, de Keizer B. Nuclear Medicine Imaging in Neuroblastoma: Current Status and New Developments. J Pers Med 2021;11:270.
8. Yanik GA, Parisi MT, Shulkin BL, Naranjo A, Kreissman SG, London WB, Villablanca JG, Maris JM, Park JR, Cohn SL, McGrady P, Matthay KK. Semiquantitative mIBG scoring as a prognostic indicator in patients with stage 4 neuroblastoma: a report from the Children's oncology group. J Nucl Med 2013;54:541-8.
9. Messina JA, Cheng SC, Franc BL, Charron M, Shulkin B, To B, Maris JM, Yanik G, Hawkins RA, Matthay KK. Evaluation of semi-quantitative scoring system for metaiodobenzylguanidine (mIBG) scans in patients with relapsed neuroblastoma. Pediatr Blood Cancer 2006;47:865-74.
10. Gauthé M, Breton M, Jehanno N, Cellier C, Michon J, Sarnacki S, Schleiermacher G, Wartski M. Prognostic impact of postoperative 123I-metaiodobenzylguanidine scintigraphy: added value of SPECT/CT and semiquantification of the uptake at the surgical site. Q J Nucl Med Mol Imaging 2020;64:131-8.
11. Gnesin S, Leite Ferreira P, Malterre J, Laub P, Prior JO, Verdun FR. Phantom Validation of Tc-99m Absolute Quantification in a SPECT/CT Commercial Device. Comput Math Methods Med 2016;2016:4360371.
12. Duncan I, Ingold N. The clinical value of xSPECT/CT Bone versus SPECT/CT. A prospective comparison of 200 scans. Eur J Hybrid Imaging 2018;2:4.
13. Tabotta F, Jreige M, Schaefer N, Becce F, Prior JO, Nicod Lalonde M. Quantitative bone SPECT/CT: high specificity for identification of prostate cancer bone metastases. BMC Musculoskelet Disord 2019;20:619.
14. Lin L, Zheng R, Geng J, Wang X, Li M, Fan R, Zheng Y, Yang K. Skeletal standardized uptake values obtained using quantitative SPECT/CT for the detection of bone metastases in patients with lung adenocarcinoma. Front Med (Lausanne) 2023;10:1119214.
15. Ikeda T, Kitajima K, Tsuchitani T, Takahashi Y, Hama Y, Kotura N. Effectiveness of quantitative bone SPECT/CT for bone metastasis diagnosis. Hell J Nucl Med 2022;25:253-9.
16. Sun Q, Chen Y, Jin Q, Yuan X. A nomogram for predicting recurrence-free survival of intermediate and high-risk neuroblastoma. Eur J Pediatr 2022;181:4135-47.
17. Brodeur GM, Pritchard J, Berthold F, Carlsen NL, Castel V, Castelberry RP, De Bernardi B, Evans AE, Favrot M, Hedborg F. Revisions of the international criteria for neuroblastoma diagnosis, staging, and response to treatment. J Clin Oncol 1993;11:1466-77.
18. Liu J, Li C, Yang X, Lu X, Zhang M, Qian L, Wang W, Kan Y, Yang J. The Diagnostic Value of (18)F-FDG PET/CT Bone Marrow Uptake Pattern in Detecting Bone

Marrow Involvement in Pediatric Neuroblastoma Patients. Contrast Media Mol Imaging 2022;2022:7556315.
19. Ponzoni M, Bachetti T, Corrias MV, Brignole C, Pastorino F, Calarco E, Bensa V, Giusto E, Ceccherini I, Perri P. Recent advances in the developmental origin of neuroblastoma: an overview. J Exp Clin Cancer Res 2022;41:92.
20. DuBois SG, Macy ME, Henderson TO. High-Risk and Relapsed Neuroblastoma: Toward More Cures and Better Outcomes. Am Soc Clin Oncol Educ Book 2022;42:1-13.
21. Liu S, Yin W, Lin Y, Huang S, Xue S, Sun G, Wang C. Metastasis pattern and prognosis in children with neuroblastoma. World J Surg Oncol 2023;21:130.
22. Yanik GA, Parisi MT, Naranjo A, Nadel H, Gelfand MJ, Park JR, Ladenstein RL, Poetschger U, Boubaker A, Valteau-Couanet D, Lambert B, Castellani MR, Bar-Sever Z, Oudoux A, Kaminska A, Kreissman SG, Shulkin BL, Matthay KK. Validation of Postinduction Curie Scores in High-Risk Neuroblastoma: A Children's Oncology Group and SIOPEN Group Report on SIOPEN/HR-NBL1. J Nucl Med 2018;59:502-8.
23. Utnes P, Løkke C, Flægstad T, Einvik C. Clinically Relevant Biomarker Discovery in High-Risk Recurrent Neuroblastoma. Cancer Inform 2019;18:1176935119832910.
24. Feng L, Li S, Wang C, Yang J. Current Status and Future Perspective on Molecular Imaging and Treatment of Neuroblastoma. Semin Nucl Med 2023;53:517-29.
25. Streby KA, Parisi MT, Shulkin BL, LaBarre B, Bagatell R, Diller L, Grupp SA, Matthay KK, Voss SD, Yu AL, London WB, Park JR, Yanik GA, Naranjo A. Impact of diagnostic and end-of-induction Curie scores with tandem high-dose chemotherapy and autologous transplants for metastatic high-risk neuroblastoma: A report from the Children's Oncology Group. Pediatr Blood Cancer 2023;70:e30418.
26. Černý I, Prášek J, Kašpárková H. Superiority of SPECT/CT over planar 123I-mIBG images in neuroblastoma patients with impact on Curie and SIOPEN score values. Nuklearmedizin 2016;55:151-7.
27. Fendler WP, Melzer HI, Walz C, von Schweinitz D, Coppenrath E, Schmid I, Bartenstein P, Pfluger T. High ^{123}I-MIBG uptake in neuroblastic tumours indicates unfavourable histopathology. Eur J Nucl Med Mol Imaging 2013;40:1701-10.
28. Kupitz D, Wissel H, Wuestemann J, Bluemel S, Pech M, Amthauer H, Kreissl MC, Grosser OS. Optimization of SPECT/CT imaging protocols for quantitative and qualitative (99m)Tc SPECT. EJNMMI Phys 2021;8:57.
29. Delcroix O, Robin P, Gouillou M, Le Duc-Pennec A, Alavi Z, Le Roux PY, Abgral R, Salaun PY, Bourhis D, Querellou S. A new SPECT/CT reconstruction algorithm: reliability and accuracy in clinical routine for non-oncologic bone diseases. EJNMMI Res 2018;8:14.
30. Fahad Ullah M. Breast Cancer: Current Perspectives on the Disease Status. Adv Exp Med Biol 2019;1152:51-64.
31. Rogasch JMM, Hundsdoerfer P, Furth C, Wedel F, Hofheinz F, Krüger PC, Lode H, Brenner W, Eggert A, Amthauer H, Schatka I. Individualized risk assessment in neuroblastoma: does the tumoral metabolic activity on (123)I-MIBG SPECT predict the outcome? Eur J Nucl Med Mol Imaging 2017;44:2203-12.

Cite this article as: Wang X, Wang G, Zhou Z, Kan Y, Yang J. The value of ^{123}I-MIBG xSPECT/CT quantitative parameters in the diagnosis of bone metastasis in pediatric neuroblastoma patients. Quant Imaging Med Surg 2025;15(3):2570-2580. doi: 10.21037/qims-24-1251